ELSEVIER

Experimental Thermal and Fluid Science 25 (2001) 397–407

Experimental Thermal and Fluid Science

www.elsevier.com/locate/etfs

Blind hood effects on the compression wave generated by a train entering a tunnel

Marc Bellenoue *, Bruno Auvity, Tadashi Kageyama

Laboratoire de Combustion et de Détonique, ENSMA, Téléport 2, 1 Avenue Clément Ader, B.P. 40109, 86961 Futuroscope Chasseneuil du Poitou Cedex, France

Received 16 January 2001; accepted 22 July 2001

Abstract

The running of high-speed trains on railway networks creates strong transient flows in tunnels. A large number of solutions have been proposed to reduce the amplitude of the pressure gradients in tunnels and one of the most efficient solutions consists in the addition of a hood before the tunnel entrance. The present paper provides a detailed experimental study on the effects of blind hood (hood without any perforation) with constant section on the generation of a compression wave. An axisymmetric reduced scale (1/140th) experimental apparatus was used and the train Mach number was in the range from 0.06 to 0.15. Results showed that the initial compression front can be split into several smaller fronts in the presence of a blind hood. The number of fronts depends on the respective length of the hood to the train nose length and only slightly on the train Mach number. The characteristics of each of these fronts (amplitude and gradient) can be predicted for given train, tunnel and hood. Furthermore the present analysis showed that, for a fixed train/tunnel blockage ratio, there exists a unique optimum hood for which the pressure gradient can be minimized. For the usual train/tunnel blockage ratio (around 0.2), the maximum reduction of the pressure gradient was proved not to exceed 3. The exact value of the optimum pressure gradient depends on both the train/tunnel blockage ratio and the train nose geometry.

1. Introduction

The train entry into a tunnel generates an exiting flow at the portal with a direction opposite to the train movement [1,2] and a compression wave that propagates into the tunnel at the speed of sound. Developments of high-speed trains have generated numerous engineering problems related to the presence of strong compression waves in tunnels. The high amplitude of compression waves provokes strong mechanical stresses on the train body and the associated high pressure gradients are responsible for both the aural discomfort of train passengers and the impulsive acoustical wave called the *micro-pressure wave* emitted in the surrounding area of tunnel exits. The micro-pressure wave is similar to the aeronautical sonic boom and caused serious environmental damages in Japan [3].

Since the three last decades, many efforts have been dedicated to the reduction of nuisances created by high-speed trains entering tunnels. So far, no solution was found to reduce the amplitude of compression waves, except in the case of tunnels in shallow ground for which the installation of shafts is possible [4]. However, concerning the alleviation of pressure gradients, numerous solutions have been proposed and they can be grouped in two different classes. The first category concerns the solutions modifying the generation process of the compression wave. For given train/tunnel blockage ratio and train speed, the maximum amplitude of the compression wave is fixed. Then the purpose of the first category solutions is to increase the pressure rise time. It can be done either by modifying the train nose design [5,6] or the tunnel portal design [7–9]. In the latter case, a hood is placed before the tunnel entrance. It is a short region compared to the overall tunnel length and it has a bigger cross-sectional area than the tunnel itself. It can be continuously or discontinuously connected to the tunnel, with or without air vent holes. The second category solutions tend to alter the shape of the compression wave front during its propagation. Devices are placed along the tunnel to split the initial compression wave into several weaker ones. They can be open or closed side branches or parts of the tunnel

* Corresponding author. Tel.: +33-5-49-49-80-99; fax: +33-5-49-49-81-76.

E-mail address: bellenoue@lcd.ensma.fr (M. Bellenoue).

0894-1777/01/$ - see front matter
PII: S0894-1777(01)00088-7

Nomenclature

c	chosen value for the criterion used to detect the presence of a compression front
c_0	sound speed at the atmospheric conditions
C_p	non-dimensional pressure
$C_{p\,i}$	non-dimensional pressure amplitude of the ith front
C_{pmax}	maximum amplitude of the non-dimensional pressure of the whole front
D_h	hood diameter
D_{tunnel}	tunnel diameter
K	ratio of the non-dimensional amplitude of the third front and that of the second front
K_{gr}	non-dimensional pressure gradient
$K_{gr\,i}$	maximum of the non-dimensional pressure gradient for the ith front
K_{grmax}	maximum of the non-dimensional pressure gradient of the whole front
L_{front}	spatial thickness of the compression front
L_{front0}	spatial thickness of the compression front formed without hood
L_h	hood length
L_{ht1}	first transition length
L_{ht2}	second transition length
L_{nose}:	train nose length
L_{ref}	reference length (equal to the train nose length)
M	train Mach number
p	pressure
p_0	pressure at the atmospheric conditions
r	hood/tunnel sectional area ratio
S_1	sum of the non-dimensional amplitudes of the second and the third fronts
S_2	sum of the non-dimensional amplitudes of the three compression fronts
t	physical time
t_1	time needed by the train to go from the hood entrance to the tunnel entrance
t_2	time needed by the pressure information to go back and forth from the tunnel entrance to the hood entrance
t_a	non-dimensional time
$t_{aC_p\,max}$	non-dimensional time corresponding to C_{pmax}
t_c	pressure propagation time from hood entrance to pressure transducer position
t_{front}	non-dimensional duration of the compression front
V_{train}	train speed
X_μ	position of the microphone
α_i	coefficients in Eq. (8)
β	ratio of the aerodynamic train nose length and the train nose length
ρ_0	density in the atmospheric conditions
σ_h	train/hood blockage ratio
σ_t	Train/tunnel blockage ratio

with bigger sectional area to create an acoustic impedance change [3]. Besides, effects of tunnel wall surface were found to be of importance during the compression wave propagation. In case of long tunnels, compression front tends to steepen with slab tracks while they tend to thicken with ballast tracks [10]. Aoki et al. [11,12] provided a detailed experimental study on the phenomena involved in the deformation process of the compression wave front.

A large number of solutions of the first and second categories have been tested at full-scale, at reduced-scale and by means of numerical computations. The addition of a hood with vent holes placed before the tunnel entrance has been shown to be one of the most efficient solutions to reduce pressure gradients in tunnel [7]. However a more complete understanding of the main phenomena controlling the generation of the compression wave in this configuration is still needed. This paper studied in detail the effects of blind hood (without hole) with a constant section on the compression wave generation. It constitutes the generic configuration of additional hood methods. Using a simplified axisymmetric experimental apparatus, an experimental study was undertaken to examine the influence of the main train and tunnel parameters. Section 2 describes the reduced-scale experimental apparatus. Section 3 presents the results and Section 4 is dedicated to an extended discussion.

2. Experimental apparatus

Results presented in this study were obtained using an axisymmetric 1/140th experimental device, see Fig. 1. The circular cylinder train model was 600 mm in length and 25 mm in diameter. The train nose and train tail geometries were fixed: the train nose was $L_{nose} = 40$ mm long with an elliptic shape and the train tail was flat. The train model was launched by an elastic-bundle-catapult and guided on a 0.8 mm diameter wire monorail. This system was able to reach a train speed of 50 m/s (Mach number equal to 0.15). Aluminium stripes were positioned 10 mm apart along 190 mm length of the black train body. Alternating step signals generated by the reflection of an incident beam on the stripes allowed the determination of train acceleration and speed stabilization. There was no measurable deceleration of the train during the entry. The train speed was measured with an uncertainty lower than 2%.

To get different train/tunnel blockage ratios σ_t (train sectional area divided by tunnel sectional area), two tubes with different inner diameters D_{tunnel}, were used: $\sigma_t = 0.21$ for which $D_{tunnel} = 54$ mm and $\sigma_t = 0.32$ with $D_{tunnel} = 44$ mm. The tunnel length was 5.5 m. This length prevented the interaction of the observed phenomena with the depression wave reflected back from the tunnel exit.

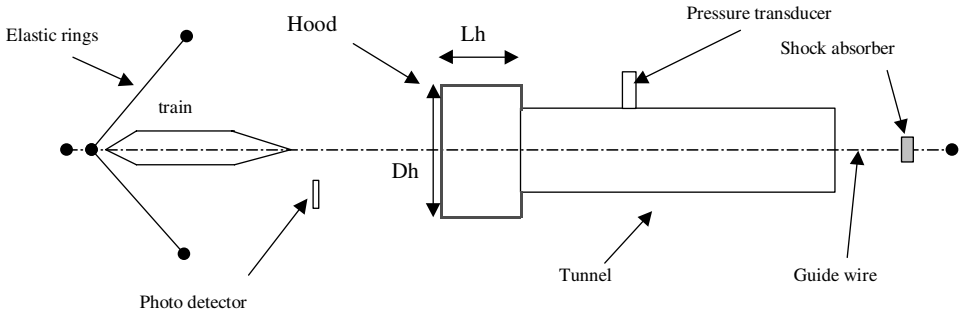

Fig. 1. Schematic of the experimental apparatus.

Compression waves were measured with a Bruel et Kjaer 1/4 in. microphone associated with a conditioner amplifier Nexus type 2690 0S4. The measurement range of the transducer was 1 psi (6900 Pa). For the highest train/tunnel blockage ratio and the highest train speed considered in this study, the maximum pressure amplitude was 1700 Pa. For this amplitude, the cumulated relative error precision for pressure measurement was lower than 1%. The sensitive surface of the microphone was mounted flush to the inner tunnel surface. To make sure that the measured pressure wave was mono-dimensional, the distance between the tunnel entrance and the microphone, X_μ, was chosen equal to $6 \times D_{\text{tunnel}}$. The pressure variation is presented using the non-dimensional pressure C_p defined as

$$C_p = \frac{p - p_0}{(1/2)\rho_0 V_{\text{train}}^2} \tag{1}$$

with p_0 and ρ_0, the pressure and the density at the atmospheric conditions and V_{train} the train speed.

A non-dimensional time scale t_a is defined as follows:

$$t_a = \frac{V_{\text{train}} \times (t - t_c)}{L_{\text{ref}}}, \tag{2}$$

where L_{ref} is a reference length chosen equal to the train nose length ($L_{\text{ref}} = L_{\text{nose}} = 40$ mm) and t_c is the time needed by the information to propagate from the hood entrance to the transducer position, $t_c = (L_h + X_\mu)/c_0$.

It has been recently proved [13] that both the parameters C_p and t_a are similitude parameters between full-scale and reduced-scale data for the problem of the compression wave generation. For identical blockage ratio σ_t and train speed V_{train}, identical compression waves are obtained at full-scale and at reduced-scale using the non-dimensional coordinates (C_p, t_a). Hence, they are called non-dimensional compression waves. The non-dimensional pressure gradient is therefore defined as

$$K_{gr} = \frac{dC_p}{dt_a}. \tag{3}$$

For experiments undertaken at a given nth reduced scale, pressure gradients are n times stronger than those at full-scale. The extreme configuration of this study ($\sigma_t = 0.32$, no hood and $V_{\text{train}} = 45$ m/s) leads to a pressure gradient of 1366 kPa/s, corresponding to K_{gr} equal to 1.05, while the frequency response of the pressure transducer is 300 kHz. To achieve a good resolution for the pressure gradient measurement, pressure signals were sampled by means of a 12-bit oscilloscope at the frequency of 200 kHz. This acquisition frequency is largely enough to capture transient phenomena with typical time of 100 μs.

The present study was focused on the effects of a blind hood with constant section on the compression wave. Such a blind hood is fully defined with two parameters: its diameter D_h and its length L_h, see Fig. 1. For $\sigma_t = 0.32$ three different blind-hood diameters were tested with the following hood/tunnel sectional area ratios r: $r = 1.3$, $r = 1.5$ and $r = 1.7$. For $\sigma_t = 0.21$, only one hood/tunnel sectional ratio, $r = 1.7$, was tested. For each r, 24 different hood lengths ranging from 0 to $6 \times L_{\text{ref}}$ (increment of $L_{\text{ref}}/4$) were considered. The explored train speed ranged from 20 to 45 m/s.

3. Results

3.1. Effects of the hood length

Fig. 2 presents non-dimensional compression waves obtained for four different hood lengths ranging from $L_h = 0$ to $L_h = 6 \times L_{\text{ref}}$ for $\sigma_t = 0.32$, $r = 1.7$ and $V_{\text{train}} = 43$ m/s. Fig. 3 presents non-dimensional pressure gradients for the same conditions. For $L_h = 0$, a typical compression wave can be observed: first a strong one-step compression front is formed from $C_p = 0$ up to $C_{p\max} = 1.1$ at a non-dimensional time $t_{aC_p\max}$ of about 1.1. Here the term ($C_{p\max}$ is defined as the value of C_p corresponding to the time where the pressure gradient returns to the zero value, see Fig. 3. We define the duration of the compression front as the non-dimensional time during which $K_{gr} \geqslant 0.05 \times K_{grmax}$, where K_{grmax} is the maximum value of the pressure gradient during the compression front. Fig. 3 shows that the non-dimensional duration of the compression front is about 2. This compression front corresponds to the train nose entry into the tunnel. However, the duration of the compression front is longer than the time needed by the train nose to enter into the tunnel, namely 1. The duration of

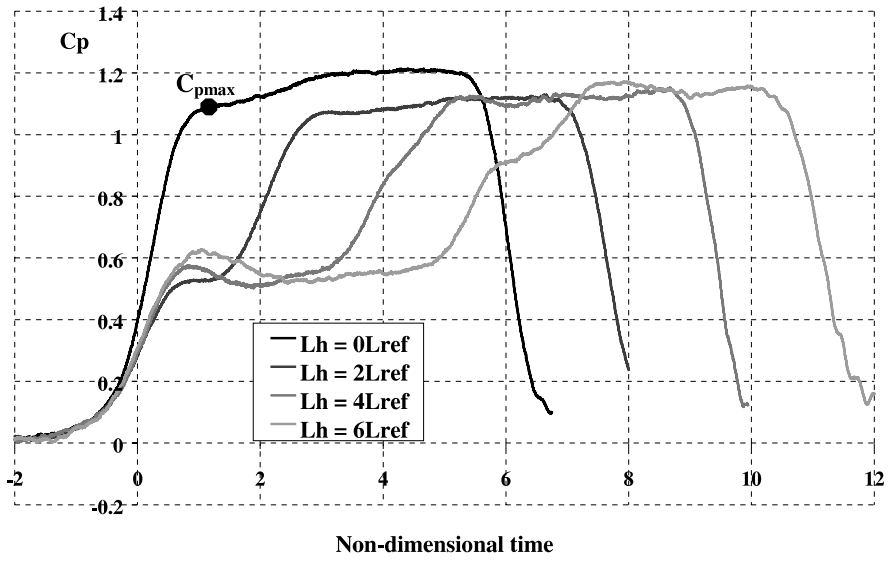

Fig. 2. Non-dimensional compression waves for different hood lengths with $\sigma_t = 0.32$, $r = 1.7$ and $V_{train} = 43.0$ m/s.

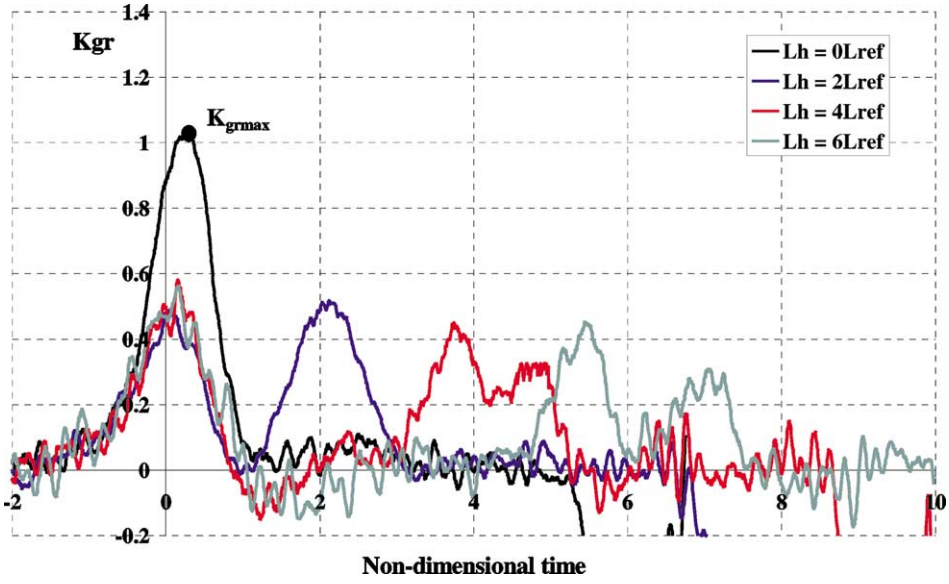

Fig. 3. Non-dimensional pressure gradients for different hood lengths with $\sigma_t = 0.32$, $r = 1.7$ and $V_{train} = 43.0$ m/s.

the compression front actually corresponds to the entry of what we will call, the "aerodynamic train nose" (ATN) in the tunnel. Note that a compression front duration of 2 means that the spatial thickness of the compression front, L_{front}, is $2 \times L_{ref}$. After $t_{aC_p\,max}$, C_p remains practically constant with a slight increase due to friction effects on train sides. Friction effects present in our reduced-scale experiments are comparable to those observable at full-scale [1]. The pressure drop that follows this phase corresponds to the passing of the train nose in front of the pressure transducer.

For $L_h = 2 \times L_{ref}$, the compression front is split into two successive steps. We can define for each of them an associated amplitude (C_{p1} and C_{p2}) and an associated maximum pressure gradient (K_{gr1} and K_{gr2}). The definition of these quantities is illustrated in Fig. 4(a) for $C_{p\,i}$ and Fig. 4(b) for $K_{gr\,i}$. After the second front, a constant pressure region similar to that observed for $L_h = 0$ is present. For $L_h = 4 \times L_{ref}$, the second front is split into two fronts. We can then define three $C_{p\,i}$ and three $K_{gr\,i}$ ($i = 1, 2, 3$). For $L_h = 6 \times L_{ref}$, the whole compression front is clearly composed of three steps. The presence of each of these fronts can be observed in Fig. 3 where a peak in the curve $K_{gr}(t_a)$ is associated to each compression front.

A criterion was introduced to determine when a new front occurs: focusing on the curve $K_{gr}(t_a)$, a new front is considered to be generated when the value of K_{gr}

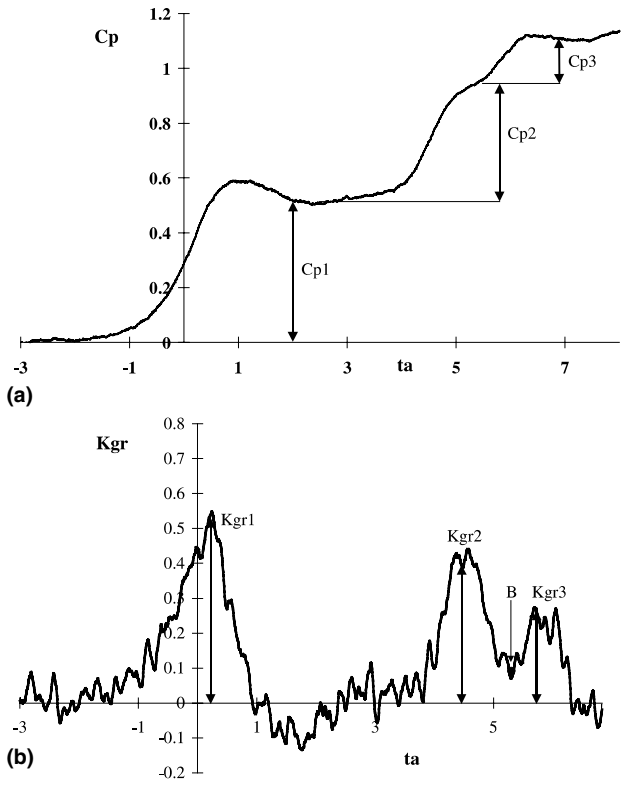

Fig. 4. (a) Definition of the quantities C_{pi}. (b) Definition of the quantities K_{gri}.

between two successive crests becomes lower than a certain percentage $\sqrt{c}$ (typically 60%) of the value of the former crest. For example, in Fig. 4(b), the value of K_{gr} at the point B has to be lower than or equal to $c \times K_{gr2}$ with $c = 0.60$. In Fig. 5, the values of C_{pi} ($i = 1, 2, 3$) are plotted for each tested hood length for $\sigma_t = 0.32$, $r = 1.7$ and $V_{train} = 43$ m/s. The values $S_1 = C_{p2} + C_{p3}$ and $S_2 = C_{p1} + C_{p2} + C_{p3}$ are also reported in Fig. 5. It is clearly shown that, for $c = 0.6$, the transition from one-step compression front to two-step compression fronts occurs when $L_h \geqslant L_{ht1} = L_{ref}$ and the transition from two-step to three-step compression fronts occurs for $L_h \geqslant L_{ht2} = 3.5 \times L_{ref}$. For $c = 0$, we obtained $L_{ht1} = 2 \times L_{ref}$ and $L_{ht2} = 6 \times L_{ref}$. Regardless of the chosen value for c, C_{p1} keeps a constant value, about 1.1, till the appearance of the second step. From this point, $L_h > L_{ht1}$, C_{p1} reaches a new value, 0.51 and stays constant. The same phenomenon takes place for C_{p2} which is constant to 0.55 up to $L_h = L_{ht2}$. From this point, C_{p2} is equal to 0.40. The values of S_1 and S_2 remain constant regardless of the hood length. This result suggests that the initial compression front generated without hood is successively split into several parts (maximum three-step front) in presence of a blind hood.

Concerning the values of K_{gri} ($i = 1, 2, 3$), a different behavior can be observed, see Fig. 6: for $L_h \leqslant L_{ht1}$, the value of K_{gr1} decreases as L_h increases. For $L_h \geqslant L_{ht1}$, the value of K_{gr1} is constant. For $L_{ht1} \leqslant L_h \leqslant L_{ht2}$, the value of K_{gr2} decreases till the appearance of the third step. For $L_h \geqslant L_{ht2}$, the value of K_{gr2} is constant. The values of C_{pi}, respectively, K_{gri}, for $\sigma_t = 0.32$ and $r = 1.7$ are reported in Table 1, respectively, Table 2, for $L_h \geqslant L_{ht2}$.

3.2. Effects of hood/tunnel sectional area ratio, r, and train/tunnel blockage ratio, σ_t

Experiments similar to those presented in Section 3.1 were repeated for $r = 1.3$ and $r = 1.5$ with $\sigma_t = 0.32$ and $V_{train} = 43$ m/s. Using the same criterion c, transitions from one-step compression front to two-step compression fronts, and transitions from two-step to three-step compression fronts occur for the same hood lengths. Therefore the splitting of the initial compression front does not depend on the hood/tunnel sectional area ratio but only on the hood length. The values of C_{pi} and K_{gri} ($i = 1, 2, 3$) are reported in Tables 1 and 2 for $L_h > L_{ht2}$ for $r = 1.3$ and $r = 1.5$. The quantity S_2 is almost

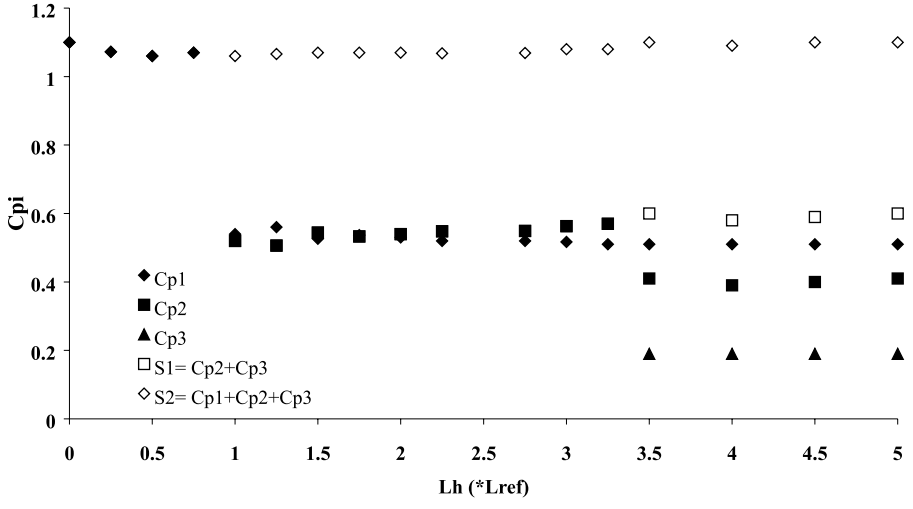

Fig. 5. Evolution of C_{pi} versus hood length with $c = 0.60$.

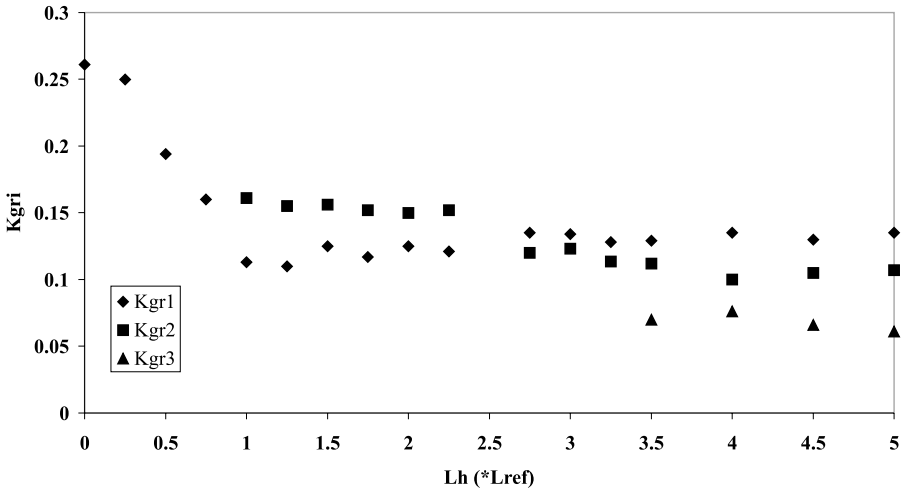

Fig. 6. Evolution of K_{gri} versus hood length with $c = 0.60$.

Table 1
Evolution of C_{p1}, C_{p2} and C_{p3} for different values of r for $\sigma_t = 0.32$ and $L_h \geqslant L_{ht2}$

	$r = 1.3$	$r = 1.5$	$r = 1.7$
C_{p1}	0.74	0.63	0.51
C_{p2}	0.29	0.34	0.40
C_{p3}	0.13	0.15	0.19
$S_2 = C_{p1} + C_{p2} + C_{p3}$	1.16	1.12	1.10

Table 2
Evolution of K_{gr1}, K_{gr2} and K_{gr3} for different values of r for $\sigma_t = 0.32$ and $L_h \geqslant L_{ht2}$

	$r = 1.3$	$r = 1.5$	$r = 1.7$
K_{gr1}	0.72	0.66	0.54
K_{gr2}	0.34	0.4	0.42
K_{gr3}	0.21	0.24	0.25

insensitive to r but all the C_{pi} are modified. C_{p1} decreases when r increases. The hood can actually be considered as the first short tunnel with its specific blockage ratio $\sigma_h = S_{train}/S_h$ and C_{p1} corresponds to the maximum amplitude of the compression wave generated by the train entry in this short tunnel. The bigger r is, the smaller σ_h is and the lower C_{p1} is. To illustrate this result, Fig. 7 presents three compression waves obtained for $r = 1.3$, 1.5 and 1.7 with $\sigma_t = 0.32, L_{ht1} < L_h = 2.0 \times L_{ref} < L_{ht2}$ and $V_{train} = 43$ m/s. The bigger r is, the bigger S_1 is as S_2 keeps a constant value equal to C_{pmax}. Interestingly, as shown in Table 3, the ratio $K = C_{p3}/C_{p2}$ does not depend on r.

In order to clarify the influence of σ_t on the compression wave generation, the same hood was tested ($r = 1.7$ and $L_{ht1} < L_h = 2.25 \times L_{ref} < L_{ht2}$) for $\sigma_t = 0.21$ and $\sigma_t = 0.32$. The maximum amplitude of the whole front obviously depends on the value of σ_t: $C_{pmax} = 0.59$ for $\sigma_t = 0.21$ and $C_{pmax} = 1.1$ for $\sigma_t = 0.32$. However, if the quantity C_p/C_{pmax} is plotted versus t_a, both the compression waves are similar, see Fig. 8. For $L_h \leqslant L_{ht2}$ (while the front is a two-step front), the train/tunnel blockage ratio does not change the pressure–time history but only modifies all the pressure levels C_{pi} with a homothetic transformation.

4. Discussion

Results shown above revealed that the initial compression front is split into two or three successive fronts in the presence of a blind hood. Let us identify the phenomena responsible for this feature using an (x,t) diagram and its associated pressure recording, see Fig. 9, corresponding to the following experimental conditions: $L_h = 6 \times L_{ref} \geqslant L_{ht2}$, $\sigma_t = 0.32$, $r = 1.7$ and $V_{train} = 43$ m/s. For clarity, dimensional coordinates of the reduced-scale test are used here. In the (x,t) diagram, the thin lines represent the compression waves and the dashed lines the expansion waves. They both propagate with the sound speed. The thick lines represent the progression of the tip and the end of the aerodynamic train nose (ATN). The use of a long hood permitted to clearly show three separated compression fronts. This fact is also visible on the $K_{gr}(t_a)$ curve, see Fig. 3, where K_{gr} returns to about zero between two successive crests.

As mentioned in Section 3.1, for $c = 0$ the first transition length is about $L_{ht1} = 2 \times L_{ref}$ regardless of the value of σ_t. This length is actually equal to the thickness of the compression front formed without a hood, L_{front0}. For a hood length higher than L_{front0}, the hood can be considered as a short tunnel and the compression front corresponding to the train entry in the hood is completely established. The lines OC1h and OC1e in Fig. 9, respectively, represent the head and the end of the first compression front OC1. The point A, respectively, point B, on the pressure–time curve Fig. 9 indicates the passing of the head (respectively, the end)

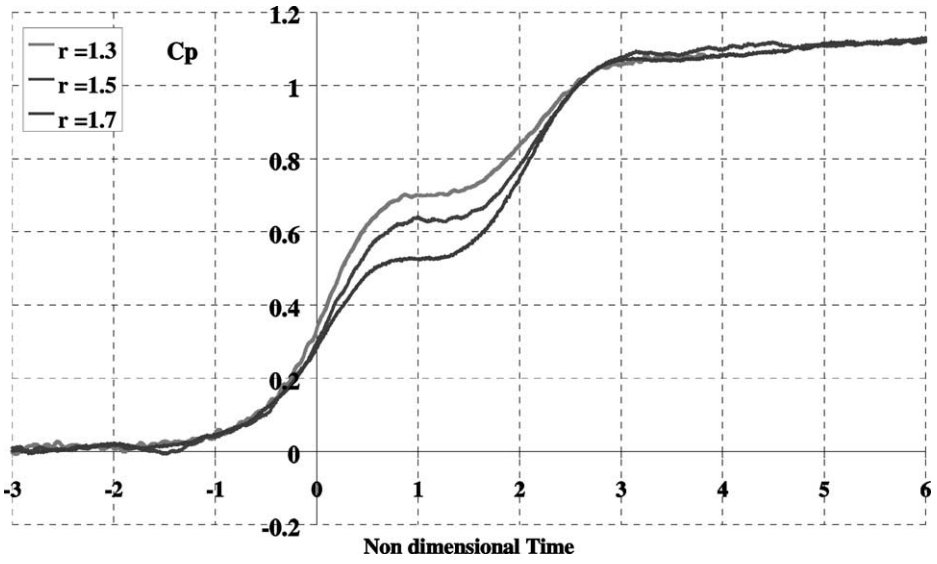

Fig. 7. Compression waves obtained for the three different ratios r with $\sigma_t = 0.32$, $L_{ht1} < L_h = 2.0 \times L_{ref} < L_{ht2}$ and $V_{train} = 43.0$ m/s.

Table 3
Evolution of $K = C_{p3}/C_{p2}$ with σ_t and r

	$r = 1.3$	$r = 1.5$	$r = 1.7$
$\sigma_t = 0.32$	0.46	0.45	0.47
$\sigma_t = 0.21$	–	–	0.625

of OC1 in front of the microphone. The compression front comprised between the point A and the point B corresponds to the entry of the ATN in the hood. Remember that the corresponding time t_{front} is not L_{nose}/V_{train} but $t_{front} = (\beta L_{nose})/V_{train}$ with β practically equal to 2 for the considered nose, see Section 3.1. This value of β depends on the train nose geometry, mainly on the train nose length, and on the train/tunnel blockage ratio [14]. When the wave OC1 reaches the tunnel entry, marked by the dashed horizontal line on the (x,t) diagram, one part of this wave reflects back toward the hood entrance as a compression wave (OC1′) and the remaining part is transmitted as a compression wave in the tunnel toward its end. Then OC1′ reflects at the hood entrance as an expansion wave (OD1). This expansion wave is responsible for the pressure decrease between points B and C. Multiple reflections of the initial compression front between the hood entrance and the tunnel entrance take place till the complete damping of these waves (for clarity, all the corresponding waves are not reported on the (x,t) diagram). To determine the amplitude of OC1′ and OD1, pressure measurements must be performed in the hood. As can be seen in the (x,t) diagram of Fig. 9, superposition of these waves occurs. To avoid this, the minimum length of the hood is $12 \times L_{ref}$ and pressure transducer must be at $X_\mu = 6 \times L_{ref}$.

When the train enters the tunnel, the section decrease creates a new compression wave in the tunnel, OC2. OC2 is responsible for the second pressure rise on the pressure–time curve. According to the results obtained by the authors in [1], an increase in the train/tunnel blockage ratio is accompanied by an increase in the mass of air pushed upstream of the train nose and by a decrease in the mass of air ejected from the tunnel. A decrease in the mass of air ejected from the tunnel is directly related to a decrease in the mass flux toward the outside of the tunnel. Then, when the train enters the tunnel, a depression wave, OD2 Fig. 9, is also generated at the tunnel entrance and propagates back to the hood entrance, to adjust the mass flux at the hood entrance. OD2 reflects back at the hood entrance as a compression wave, OC3. When OC3 reaches the tunnel entrance, one part is transmitted toward the tunnel end and is responsible for the third pressure rise on the pressure–time curve. The remaining part is reflected back to the hood entrance (OC3′) which in turn reflects as an expansion wave at the hood entrance (OD3′). The amplitude C_{p3} of the compression front OC3 is equal to the amplitude of the expansion wave OD2 and is directly related to the amplitude C_{p2} of OC2. Indeed, as Table 3 shows, the ratio $K = C_{p3}/C_{p2}$ is constant for a given σ_t and does not depend on σ_h (or r).

Each of the compression fronts corresponds to the ATN entry in the hood or in the tunnel. So the corresponding pressure-rise time t_{front} is almost identical for all of them and equal to $t_{front} = (\beta L_{nose})/V_{train}$. The time delay between the first compression front OC1 and the second front OC2 corresponds to the time t_1 needed by the train to travel from the hood entrance to the tunnel entrance, i.e. $t_1 = (L_h)/V_{train}$, see Fig. 9. Consequently, the first front is dissociated from the second front when the following relationship is satisfied:

$$t_1 = \frac{L_h}{V_{train}} > t_{front} = \frac{\beta L_{nose}}{V_{train}}. \quad (4)$$

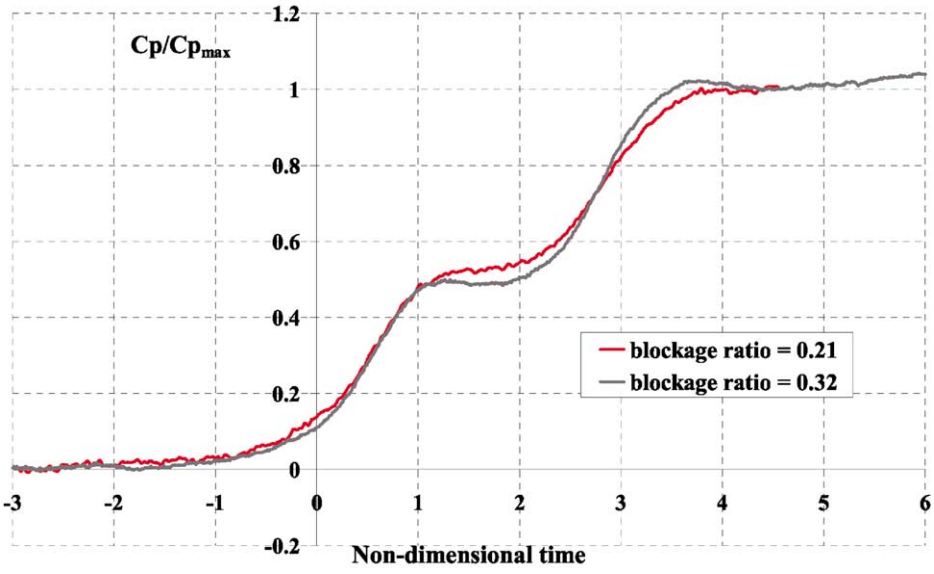

Fig. 8. Compression waves obtained for the two different blockage ratios σ_t with $r = 1.7$, $L_{ht1} < L_h = 2.25 \times L_{ref} < L_{ht2}$ and $V_{train} = 43.0$ m/s.

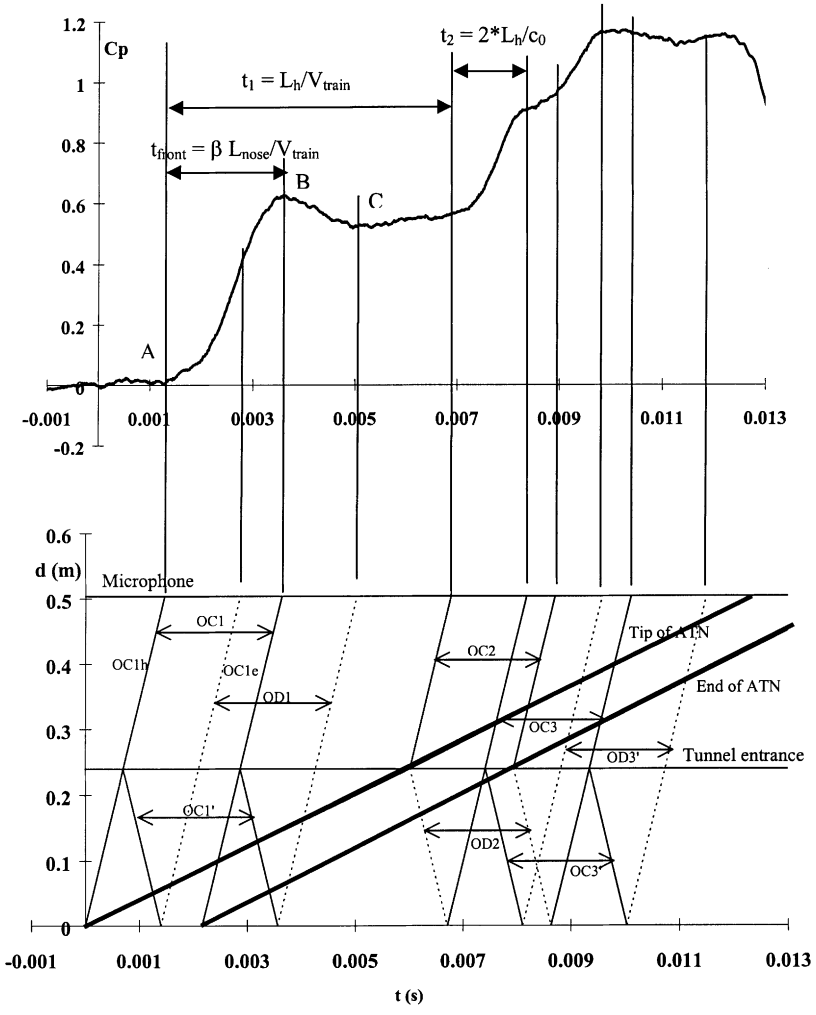

Fig. 9. (x, t) diagram for $L_h = 2.25 \times L_{ref}$, $\sigma_t = 0.32$, $r = 1.7$ and $V_{train} = 43.0$ m/s.

Eq. (4) leads to

$$\frac{L_{ht1}}{L_{ref}} = \beta. \tag{5}$$

Eq. (5) is consistent with the experimental observation of the first transition length reported in Section 3.1. The time delay between the second front OC2 and the third front OC3 corresponds to the time t_2 needed by the expansion wave OD2 to go back and forth from the tunnel entrance to the hood entrance at the sound speed c_0, i.e. $t_2 = 2L_h/c_0$. Therefore, the third front is totally dissociated from the second front when $t_2 > t_{front}$, which means

$$\frac{L_{ht2}}{L_{ref}} = \frac{\beta}{2M} \tag{6}$$

with $M = V_{train}/c_0$ the train Mach number. L_{ht2} depends on both the train nose length and the train Mach number. For $V_{train} = 20$ m/s ($M = 0.06$), $L_{ht2}/L_{ref} = 16.7$ and for $V_{train} = 43$ m/s ($M = 0.13$), $L_{ht2}/L_{ref} = 7.9$. We experimentally found a value of 6 for $c = 0$, see Section 3.1.

The presence of the first front OC1 and the second front OC2 was already reported [7,15]. However, the presence and the origin of the third compression front OC3 was never revealed before the present study. This is mainly due to the fact that perforations were often added in the case of long hoods [6]. Based on the results discussed above, the number of compression fronts can be predicted according to the hood length, for given train nose and train speed. Are the corresponding maximum amplitudes and maximum pressure gradients predictable?

The first compression front is completely formed for $L_h \geqslant L_{ht1}$ and its amplitude corresponds to the amplitude of the compression wave generated by the train entry in a tunnel with a blockage ratio equal to $\sigma_h = S_{train}/S_h$. Several semi-empirical formulations were developed to predict the maximum amplitude of the compression wave [3,16,17]. All these formulations give very similar results and we will use the one developed by Ozawa [3]:

$$C_{pmax} = f(\sigma, M) = \frac{1-(1-\sigma)^2}{(1-M)(M+(1-\sigma)^2)}. \tag{7}$$

The maximum amplitude only depends on the train/tunnel blockage ratio and the train speed. However, for $M > 0.05$ and for moderate σ ($\sigma < 0.35$), C_{pmax} is almost insensitive to the train speed and C_{pmax} can be estimated by $C_{pmax} = f(\sigma)$. For $r = 1.7$ and $\sigma_t = 0.32$, the blockage ratio of the hood becomes $\sigma_h = \sigma_t/r = 0.188$ and the predicted value by the Eq. (7) is $C_{p1} = 0.50$ (to be compared with the measured value $C_{p1} = 0.51$).

Concerning the amplitude of the second and the third compression fronts C_{p2} and C_{p3}, no formulation is available in the literature. However, the value $S_1 = C_{p2} + C_{p3}$ is known since the overall sum $S_2 = C_{p1} + C_{p2} + C_{p3}$ was found to be constant to C_{pmax}, which is fixed by σ_t. The ratio $K = C_{p3}/C_{p2}$ does not depend on r but only on σ_t, see Table 3. Hence, all the values C_{p1}, C_{p2} and C_{p3} are fixed for a given σ_t and can be predicted when the function $K(\sigma_t)$ is known. From our experiments we can deduce that $K(\sigma_t = 0.21) = 0.63$ and $K(\sigma_t = 0.32) = 0.46$.

In Fig. 10, maxima of the pressure gradient K_{gri} are reported as a function of the maximum amplitude C_{pi} ($i = 1, 2, 3$) for $L_h \geqslant L_{ht2}$. K_{grmax} and C_{pmax} corresponding to the configuration without hood are also given for $\sigma_t = 0.32$ and $\sigma_t = 0.21$. It can be seen that a linear relationship exists between K_{gr} and the associated C_p

$$K_{grmax} = \alpha_1(L_{nose})C_{pmax} + \alpha_2(L_{nose}), \tag{8}$$

where α_i is a constant which mainly depends on the train nose length and slightly on the tunnel entrance geome-

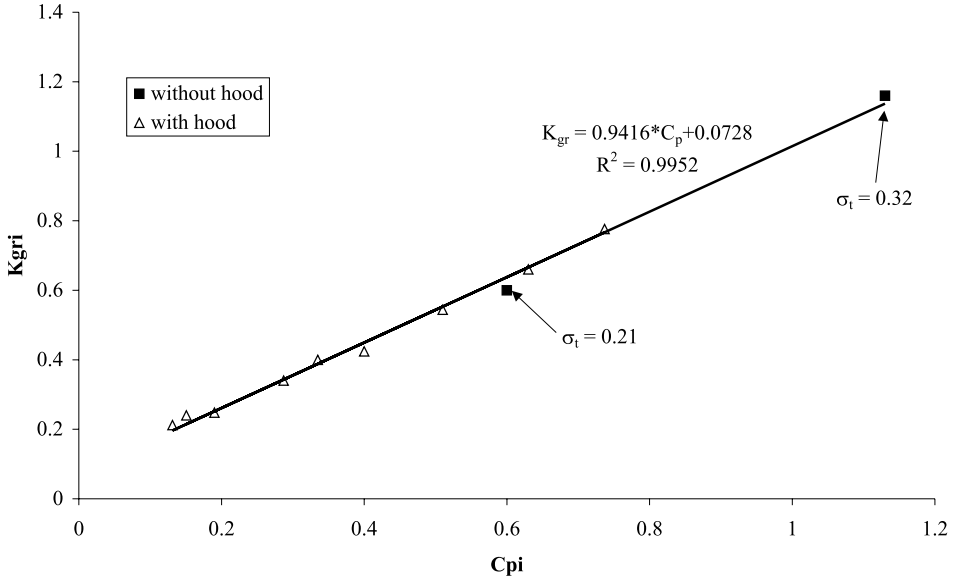

Fig. 10. Non-dimensional maximum pressure gradient K_{gri} versus non-dimensional maximum amplitude C_{pi} ($i = 1, 2, 3$).

try. A similar result was already observed in the case of a train-tunnel entry without hood [9,16]. However, this relationship is verified for all the compression fronts formed in the presence of blind hood and the proportionality coefficient, α_1, is the same for all the fronts. The lower limit of the validity of Eq. (8) is estimated to be for $C_p = 0.1$. K_{gr} must be equal to 0 when C_p reaches 0. For a given nose, α_1 can be determined with a good accuracy from only one pressure measurement with any value of σ_t.

Eq. (8) has important implications for hood design. As it has been proved that all the C_{pi} can be predicted for any blind hood, then all the associated values of maximum pressure gradient K_{gri} are known. Moreover, the present analysis shows that the value of r for which the minimum pressure gradient is reached can be determined. This value is unique for a fixed σ_t. Therefore the value of the minimum pressure gradient achievable with a constant-section blind hood can be calculated and its value only depends on σ_t and the train nose geometry. Indeed, the lowest values of K_{gri} are obtained for $L_h \geqslant L_{ht2}$, see Fig. 6. As Table 2 shows, the bigger r is, the lower K_{gr1} and the greater K_{gr2} are. Then the minimum pressure gradient is obtained for $K_{gr1} = K_{gr2}$, the value of K_{gr3} being always lower than K_{gr2}. For clarity in the following equations, we will neglect the constant α_2. C_{p1} is determined from Eq. (7), with σ_h being fixed. Then

$$K_{gr1} = \alpha(L_{nose})C_{p1} = \alpha(L_{nose})f(\sigma_h). \tag{9}$$

We also have

$$C_{p2} + C_{p3} = f(\sigma_t) - C_{p1} \tag{10}$$

and

$$\frac{C_{p3}}{C_{p2}} = K(\sigma_t). \tag{11}$$

Then, from (10) and (11)

$$K_{gr2} = \alpha(L_{nose})C_{p2} = \alpha(L_{nose})\frac{f(\sigma_t) - f(\sigma_h)}{1 + K(\sigma_t)}. \tag{12}$$

As

$$K_{gr1} = K_{gr2}. \tag{13}$$

Then σ_h that leads to the minimum pressure gradients is given by the following relationship:

$$f(\sigma_h) = \frac{f(\sigma_t)}{2 + K(\sigma_t)}. \tag{14}$$

From Eq. (14), σ_h is known and then $r = \sigma_t/\sigma_h$ is deduced. From Eq. (9), the minimum value of K_{gr1} is obtained. For example, for $\sigma_t = 0.32$, the value of r corresponding to the minimum achievable value of K_{gr1} is equal to 2.0 and the minimum value of K_{gr1} itself is 0.46 ($C_{p1} = 0.41$). For $\sigma_t = 0.21$, the optimum value of r is 2.3 and K_{gr1} is 0.28 ($C_{p1} = 0.22$).

The splitting of the initial compression front into three successive fronts is efficient to reduce the maximum pressure gradient. For example, the maximum pressure gradient is divided by 2 for $L_h = 6 \times L_{ref}$ and $r = 1.7$, see Fig. 3. However for the same hood length, a lower and optimum pressure gradient would be obtained with a flared hood for which the pressure increases linearly all along the front. In this case, the pressure gradient would be constant and an overall minimum. A flared hood can be regarded as a succession of short constant-section hoods with decreasing sections. The present analysis shows that, for a constant-section hood, the shape of the *non-dimensional* compression front rigorously depends on the train nose length for t_1 (which becomes L_h/L_{nose} in non-dimensional form), t_{front} (which becomes β in non-dimensional form) and t_2 (which becomes $2 \times L_h/L_{nose} \times M$ in non-dimensional form), and the train Mach number for t_2. Consequently, the overall compression front obtained with a flared hood depends on both these parameters. So no optimum shape design can stay valid regardless of the train Mach number and the train nose geometry. However, the dependence on the train Mach number is suggested to be very small as a flared portal is regarded as a succession of short constant section hood for which $L_h < L_{ht1}$, i.e. a succession of two-step fronts for which the shape is mainly controlled by t_1. For a train nose of the usual aspect ratio (L_{nose}/D_{train} around 2), the train nose geometry will only weakly influence the overall compression front shape. These conclusions justify that an optimum shape can be found regardless of the train speed for "snub" nose train [8].

5. Conclusion

Effects of blind hood with constant section on the generation process of compression wave due to a train-tunnel entry were examined. A reduced-scale experimental apparatus (1/140th) with an axially symmetrical geometry was used. Both the parameters defining a constant-section blind hood (diameter and length) were separately explored in order to provide an insight into the main phenomena created in the presence of it. The study revealed that, according to the respective hood length to the train nose length, the compression front can be divided into 1–3 successive fronts. The number of fronts does not depend on the hood/tunnel sectional ratio or on the train/tunnel blockage ratio. The analysis developed in the paper showed that the maximum amplitude and the maximum pressure gradient of every fronts can be predicted. Furthermore, it was shown that, for a fixed train/tunnel blockage ratio, there exists a unique optimum hood for which the pressure gradient can be minimized. The value of the minimum pressure gradient depends on both the train-tunnel blockage ratio and the train nose geometry.

The maximum efficiency $(K_{grmax})/K_{grmin}$ of a constant-section blind hood is determined by the relationship: $(K_{grmax})/K_{grmin} = 2 + K(\sigma_t)$. For usual σ_t on the high-speed railway network, σ_t is comprised between 0.1 and 0.3 and the value of $(K\sigma_t)$ is about 0.6. Therefore, the maximum efficiency of a blind hood is about 3. The only way to increase the efficiency of a hood is to add

some perforation on it [6,9] and/or to design the shape [8]. The next step in the train-tunnel entry problem will be to find countermeasures to reduce the maximum amplitude of the compression wave.

Acknowledgements

This work was supported by PREDIT 2 – AIVE (Aérodynamique instationnaire des véhicules terrestres et de leur environnement). The authors would like to acknowledge the technical assistance provided by Alain DESTOR.

References

[1] B. Auvity, M. Bellenoue, T. Kageyama, Experimental study of the unsteady aerodynamic field outside a tunnel during a train entry, Experiments in Fluids 30 (2001) 221–228.

[2] B. Auvity, M. Bellenoue, Vortex structure generated by a train-tunnel entry near the portal, in: G.M. Carlomagno, I. Grant (Eds.), Proceedings of the 8th International Symposium on Flow Visualization, Sorento, Italy, 1998.

[3] S. Ozawa, Study of micro-pressure wave radiated from a tunnel exit, Railway Technical Research Report, 1979.

[4] R.G. Gawthorpe, C.W. Pope, Reduced cross sections for high speed tunnels in shallow ground, STECH, vol. II, Yokohama, Japan, 1993, pp. 185–190.

[5] T. Maeda, T. Matsumura, M. Iida, et al., Effect of shape of train nose on compression wave generated by train entering tunnel, in: International Conference on Speedup Technology for Railway and Maglev Vehicles, Yokohama, Japan, 1993, pp. 315–319, November 22–26.

[6] S. Ozawa, T. Maeda, T. Matsumura, K. Uchida, Micro-pressure waves radiating from exits of Shinkansen tunnels, Quartely Reports of RTRI 34 (2) (1993) 134–140.

[7] S. Ozawa, T. Maeda, T. Matsumura, et al., Countermeasures to reduce micro-pressure waves radiating from exits of Shinkansen tunnels, in: 7th International Symposium on Aerodynamics and Ventilation of Vehicle Tunnels, Brighton, UK, 1991.

[8] M.S. Howe, On the compression wave generated when a high-speed train enters a tunnel with a flared portal, Journal of Fluids and Structures 13 (1999) 481–498.

[9] M. Bellenoue, T. Kageyama, Train/tunnel geometry on the compression wave generated by a high-speed train, in: B. Schulte-Werning, R. Gregoire, A. Malfatti, G. Matschke (Eds.), TRANSAERO – A European Initiative on Transient Aerodynamics for Railway System Optimisation, Results of the Brite/Euram Project "Transient Aerodynamics for Railway System Optimisation", Notes on Numerical Fluid Mechanics, Springer, Berlin, 2001, to appear.

[10] S. Ozawa, T. Maeda, T. Matsumura, K. Uchida, Effect of ballast on pressure wave propagating through tunnel, in: International Conference on Speedup Technology for Railway and Maglev Vehicles, Yokohama, Japan, 1993, November 22–26.

[11] T. Aoki, K. Matsuo, H. Hidaka, et al., Attenuation and distorsion of propagating compression waves in a high-speed railway model and in a real tunnel, in: 20th International Symposium on Shock Waves, Marseille, France, 1995.

[12] T. Aoki, N. Kondoh, K. Matsuo, S. Mashimo, Transition of unsteady boundary layer induced by propagation compression wave, in: 20th International Symposium on Shock Waves, Marseille, France, 1995.

[13] M. Bellenoue, T. Kageyama, Reduced-scale simulation of the compression wave generated by the entry of a high-speed train into a tunnel, in: B. Schulte-Werning, R. Gregoire, A. Malfatti, G. Matschke (Eds.), TRANSAERO – A European Initiative on Transient Aerodynamics for Railway System Optimisation, Results of the Brite/Euram Project "Transient Aerodynamics for Railway System Optimisation", Notes on Numerical Fluid Mechanics, Springer, Berlin, 2001, to appear.

[14] B. Auvity, Phénomènes aérodynamiques instationnaires générées par l'entrée d'un train dans un tunnel, Ph.D. Dissertation of the University of Poitiers, 1998.

[15] B. Auvity, T. Kageyama, Etude expérimentale et numérique de l'onde de compression générée par l'entrée d'un train dans un tunnel, CRAS Paris, t. 323, Série IIb, Mécanique des Fluides, 1996, pp. 87–94.

[16] K. Matsuo, T. Aoki, S. Mashimo, E. Nakastu, Entry compression wave generated by a high-speed train entering a tunnel, in: 9th Aerodynamics and Ventilation of Vehicle Tunnels, BHR Group Conference Series Publication, 27, 1997, pp. 925–934, ISBN 1 86058 0920.

[17] R. Gregoire, J.M. Réty, F. Masbernat, et al., Experimental study (scale 1/70th) and numerical simulations of the generation of pressure waves and micro-pressure waves due to high-speed train-tunnel entry, in: 9th International Symposium on Aerodynamics and Ventilation of Vehicle Tunnels, Aosta Valley, Italy, 1997.